

Lattice configurations in spin-1 Bose-Einstein condensates with the SU(3) spin-orbit coupling

Ji-Guo Wang(王继国), Yue-Qing Li(李月晴), Yu-Fei Dong(董雨菲)

Citation: Chin. Phys. B . 2020, 29(10): 100304 . **doi:** 10.1088/1674-1056/abab72
Journal homepage: http://cpb.iphy.ac.cn; http://iopscience.iop.org/cpb

What follows is a list of articles you may be interested in

Interference properties of two-component matter wave solitons

Yan-Hong Qin(秦艳红), Yong Wu(伍勇), Li-Chen Zhao(赵立臣), Zhan-Ying Yang(杨战营)

Chin. Phys. B . 2020, 29(2): 020303 . **doi:** 10.1088/1674-1056/ab65b7

Trapped Bose-Einstein condensates with quadrupole-quadrupole interactions

An-Bang Wang(王安邦), Su Yi(易俗)

Chin. Phys. B . 2018, 27(12): 120307 . **doi:** 10.1088/1674-1056/27/12/120307

Tunable ground-state solitons in spin-orbit coupling Bose-Einstein condensates in the presence of optical lattices

Huafeng Zhang(张华峰), Fang Chen(陈方), Chunchao Yu(郁春潮), Lihui Sun(孙利辉), Dahai Xu(徐大海)

Chin. Phys. B . 2017, 26(8): 080304 . **doi:** 10.1088/1674-1056/26/8/080304

Generating periodic interference in Bose-Einstein condensates

Shen-Tong Ji(冀慎统), Yuan-Sheng Wang(王元生), Yue-E Luo(罗月娥), Xue-Shen Liu(刘学深)

Chin. Phys. B . 2016, 25(9): 090303 . **doi:** 10.1088/1674-1056/25/9/090303

Three-dimensional solitons in two-component Bose-Einstein condensates

Liu Yong-Kai, Yang Shi-Jie

Chin. Phys. B . 2014, 23(11): 110308 . **doi:** 10.1088/1674-1056/23/11/110308

Lattice configurations in spin-1 Bose–Einstein condensates with the SU(3) spin–orbit coupling*

Ji-Guo Wang(王继国)[1,2,†], Yue-Qing Li(李月晴)[1,2], and Yu-Fei Dong(董雨菲)[1,2]

[1] *Department of Mathematics and Physics, Shijiazhuang TieDao University, Shijiazhuang* 050043, *China*
[2] *Institute of Applied Physics, Shijiazhuang TieDao University, Shijiazhuang* 050043, *China*

(Received 6 April 2020; revised manuscript received 2 July 2020; accepted manuscript online 1 August 2020)

We consider the SU(3) spin–orbit coupled spin-1 Bose–Einstein condensates in a two-dimensional harmonic trap. The competition between the SU(3) spin–orbit coupling and the spin-exchange interaction results in a rich variety of lattice configurations. The ground-state phase diagram spanned by the isotropic SU(3) spin–orbit coupling and the spin–spin interaction is presented. Five ground-state phases can be identified on the phase diagram, including the plane wave phase, the stripe phase, the kagome lattice phase, the stripe-honeycomb lattice phase, and the honeycomb hexagonal lattice phase. The system undergoes a sequence of phase transitions from the rectangular lattice phase to the honeycomb hexagonal lattice phase, and to the triangular lattice phase in spin-1 Bose–Einstein condensates with anisotrpic SU(3) spin–orbit coupling.

Keywords: Bose–Einstein condensates, lattice configurations, SU(3) spin–orbit coupling

PACS: 03.75.Lm, 03.75.Mn, 67.85.Hj, 67.80.K– **DOI:** 10.1088/1674-1056/abab72

1. Introduction

The experimental realization of the artificial Abelian or non-Abelian gauge potential in neutral atoms[1,2] gives rise to the spin–orbit coupling (SOC) effect in the ultracold atoms. The one-dimensional (1D) and two-dimensional (2D) SOC effects have been experimentally realized in Bose–Einstein condensates (BECs) or ultracold Fermi gases.[3–8] It is well-known that the plane wave phase, the stripe phase, and the meron with dipole–dipole repulsion[9–13] can be generated in spin–orbit coupled spin-1/2 BECs depending on the relative magnitude of intraspecies and interspecies interactions. The realization of SOC in experiment also brings a completely new avenue for the study of the many-body dynamics of the spin–orbit coupled BECs. The dark and bright solitons, quantized vortices dynamics, and Josephson dynamics are also studied in spin–orbit coupled spin-1/2 BECs.[14–20]

In the spinor BECs, the complex atomic interactions give rise to many exotic ground states. For the spin-1 BECs, the mean-field ground state is a polar state with repulsive spin–spin interaction (such as ^{23}Na) and ferromagnetic state with attractive spin–spin interaction (such as ^{87}Rb).[21] For the spin-2 BECs, due to the density–density, spin–spin, and spin–singlet pair terms, the mean-field ground state exhibits a rich phase diagram mainly comprised of the ferromagnetic, uniaxial nematic (UN), biaxial nematic (BN), and cyclic states.[22–24] The spin–orbit coupled BECs with spin larger than 1/2 also have been studied in theory and experiment.[8,25] Recently, the spin–orbit coupled spinor BECs have been attained through Raman coupling among the hyperfine states or the gradient magnetic field in experiment,[26,27] which provides an interesting avenue to explore the high-spin systems with the SOC effect. The exotic ground states, phase transitions, spin squeezing, and solitons are revealed in the spin–orbit coupled spin-1 BECs.[28–38] The square lattice phase, triangular lattice phase, and vector solitons are found in the spin–orbit coupled spin-2 BECs.[39–44] In the spin–orbit coupled spin-1 BECs, most researches restricted on the SU(2) type SOC, i.e., the internal states are coupled to their momenta via the SU(2) Pauli matrices. However, the SU(2) spin matrices cannot couple the internal states $|1\rangle$ and $|-1\rangle$ in the spin-1 BECs directly. The SU(3) SOC with the spin operator spanned by the Gell–Mann matrices can completely describe the internal couplings of the spin–orbit coupled spin-1 Bose gases. The spiral spin textures, the double-quantum spin vortices, solitons, and threefold-degenerate plane wave with nontrivial spin textures were predicted in the SU(3) spin–orbit coupled Bose gases.[45–49]

In this paper, we investigate the ground-state phases of isotropic and anisotropic SU(3) spin–orbit coupled spin-1 BECs in a 2D harmonic trap respectively. The competition between the SU(3) SOC and the spin–spin interaction results in a rich variety of lattice configurations. The ground-state phase diagram spanned by the isotropic SU(3) SOC and the spin–spin interaction is presented. Five ground-state phases can be identified on the phase diagram, including the plane wave (PW) phase, the stripe (ST) phase, the kagome lattice (KL) phase, the stripe-honeycomb lattice (SHL) phase, and the honeycomb hexagonal lattice (HHL) phase. The system undergoes a sequence of phase transitions from the rectangu-

*Project supported by the National Natural Science Foundation of China (Grant No. 11904242) and the Natural Science Foundation of Hebei Province, China (Grant No. A2019210280).

†Corresponding author. E-mail: wangjiguo@stdu.edu.cn

© 2020 Chinese Physical Society and IOP Publishing Ltd

lar lattice (RL) phase to the HHL phase, and to the triangular lattice (TL) phase in the spin-1 BECs with anisotrpic SU(3) SOC.

The paper is organized as follows. In Section 2, we introduce the model of 2D SU(3) spin–orbit coupled spin-1 BECs in a harmonic trap. In Section 3, we display the ground-state phases of 2D spin-1 BECs with isotropic and anisotropic SU(3) SOCs, respectively. The PW phase, the ST phase, the KL phase, the SHL phase, and the HHL phase are found with isotropic SU(3) SOC in Subsection 3.1. The RL phase, the HHL phase, and the TL phase are found with anisotropic SU(3) SOC in Subsection 3.2. A summary is included in Section 4.

2. Model and Hamiltonian

We study the ground-state phases of the SU(3) spin–orbit coupled spin-1 BECs in a 2D harmonic trap. The expectation value of the Hamiltonian is given as

$$E[\Psi] \equiv \langle \hat{H} \rangle = \int \mathrm{d}\boldsymbol{r} \Psi_j^* \Big\{ \Big(-\frac{\hbar^2}{2m}\nabla^2 + V(\boldsymbol{r}) + \upsilon_{\mathrm{soc}} \Big) \Psi_j + \frac{1}{2}c_0 n^2 + \frac{1}{2}c_2 |\boldsymbol{F}|^2 \Big\}, \tag{1}$$

where Ψ_j $(j = 0, \pm 1)$ is the spinor wave function of the atoms condensed in the spin state $|F = 1,\ m_F = j\rangle$, m is the atomic mass, and $\boldsymbol{r} = (x, y)$. The atom density is $n = \sum_{j=1,0,-1} \Psi_j^*(\boldsymbol{r})\Psi_j(\boldsymbol{r})$ and the total atom density is $N = \int n(\boldsymbol{r})\mathrm{d}\boldsymbol{r}$. The spin density vector $\boldsymbol{F} = (F_x, F_y, F_z)$ is expressed as[50] $F_x = \frac{1}{\sqrt{2}}[\Psi_1^*\Psi_0 + \Psi_0^*(\Psi_1 + \Psi_{-1}) + \Psi_{-1}^*\Psi_0], F_y = \frac{i}{\sqrt{2}}[-\Psi_1^*\Psi_0 + \Psi_0^*(\Psi_1 - \Psi_{-1}) + \Psi_{-1}^*\Psi_0]$, and $F_z = |\Psi_1|^2 - |\Psi_{-1}|^2$. The density–density interaction $c_0 = \frac{4}{3}\hbar^2\pi(2a_2 + a_0)/m$ and the spin–spin interaction $c_2 = \frac{4}{3}\hbar^2\pi(a_2 - a_0)/m$ are given in terms of the s-wave scattering length a_0 and a_2 for atoms with total spins 0 and 2, respectively. The SU(3) SOC $\upsilon_{\mathrm{soc}} = \gamma_x\lambda_x k_x + \gamma_y\lambda_y k_y$, where k_x (k_y) and γ_x (γ_y) are the momentum and the SOC strength along the x (y) direction, respectively. The SU(3) spin matrices (λ_x, λ_y) can be expressed by the generator of the SU(3) group, i.e. the Gell–Mann matrices. Here

$$\lambda_x = \begin{pmatrix} 0 & 1 & 1 \\ 1 & 0 & 1 \\ 1 & 1 & 0 \end{pmatrix}, \quad \lambda_y = \begin{pmatrix} 0 & -\mathrm{i} & \mathrm{i} \\ \mathrm{i} & 0 & -\mathrm{i} \\ -\mathrm{i} & \mathrm{i} & 0 \end{pmatrix}. \tag{2}$$

The time evolution of the mean field is governed by

$$\mathrm{i}\hbar\frac{\partial \Psi_j}{\partial t} = \frac{\delta E}{\delta \Psi_j^*}. \tag{3}$$

We can obtain three coupled time-dependent Gross–Pitaevskii (GP) equations by substituting Eq. (1) into Eq. (3),

$$\begin{aligned}
\mathrm{i}\hbar\frac{\partial \Psi_{-1}}{\partial t} &= \Big(-\frac{\hbar^2}{2m}\nabla^2 + V(\boldsymbol{r}) \Big) \Psi_{-1} + (c_0 n - c_2 F_z)\Psi_{-1} \\
&\quad + \frac{c_2}{\sqrt{2}}F_+\Psi_0 - \hbar\Big(\gamma_y\frac{\partial}{\partial y} + \mathrm{i}\hbar_x\frac{\partial}{\partial x}\Big)\Psi_0 \\
&\quad + \hbar\Big(\gamma_y\frac{\partial}{\partial y} - \mathrm{i}\hbar_x\frac{\partial}{\partial x}\Big)\Psi_1; \\
\mathrm{i}\hbar\frac{\partial \Psi_0}{\partial t} &= \Big(-\frac{\hbar^2}{2m}\nabla^2 + V(\boldsymbol{r}) \Big) \Psi_0 + (c_0 n)\Psi_0 + \frac{c_2}{\sqrt{2}}F_-\Psi_{-1} \\
&\quad + \frac{c_2}{\sqrt{2}}F_+\Psi_1 + \hbar\Big(\gamma_y\frac{\partial}{\partial y} - \mathrm{i}\hbar_x\frac{\partial}{\partial x}\Big)\Psi_{-1} \\
&\quad - \hbar\Big(\gamma_y\frac{\partial}{\partial y} + \mathrm{i}\hbar_x\frac{\partial}{\partial x}\Big)\Psi_1; \\
\mathrm{i}\hbar\frac{\partial \Psi_1}{\partial t} &= \Big(-\frac{\hbar^2}{2m}\nabla^2 + V(\boldsymbol{r}) \Big) \Psi_1 + (c_0 n + c_2 F_z)\Psi_1 \\
&\quad + \frac{c_2}{\sqrt{2}}F_-\Psi_0 - \hbar\Big(\gamma_y\frac{\partial}{\partial y} + \mathrm{i}\hbar_x\frac{\partial}{\partial x}\Big)\Psi_{-1} \\
&\quad + \hbar\Big(\gamma_y\frac{\partial}{\partial y} - \mathrm{i}\hbar_x\frac{\partial}{\partial x}\Big)\Psi_0,
\end{aligned} \tag{4}$$

where $F_\pm = F_x \pm \mathrm{i}F_y$.

The momentum distribution of the ground-state phase can be derived from the Fourier transformation

$$|\Psi_j(\boldsymbol{k})|^2 = \Big| \int \mathrm{d}\boldsymbol{r} \exp(-\mathrm{i}\boldsymbol{k}\cdot\boldsymbol{r})\Psi_j(\boldsymbol{r}) \Big|^2. \tag{5}$$

The single-particle energy spectrum of isotropic SU(3) spin–orbit coupled spin-1 BECs in a homogeneous space has three discrete minima locating on the vertices of an equilateral triangle. The energy band structure means that the system can have the three-fold-degenerate many-body magnetized states or topologically nontrivial lattice states.[47,48] The competition between the spin–spin interaction and the SU(3) SOC results in the exotic lattice configurations.

In our paper, we introduce a 2D harmonic trap $V(\boldsymbol{r}) = m\omega^2/2(x^2 + y^2)$ to simulate the realistic devices of ultracold atomic experiments. We set $\gamma_x = \gamma$ and $\gamma_y = \zeta\gamma_x = \zeta\gamma$, where the coefficient ζ is the SOC strength ratio between γ_y and γ_x. The length (x, y) is normalized by $l = \sqrt{\hbar/(m\omega)}$. In this unit, the units of the SOC (γ) and interaction $(c_0,\ c_2)$ are $l\omega$ and $\hbar\omega l^3/N$, respectively. The density–density interaction is fixed at $c_0 = 50$.

3. Numerical results

We study the ground-state phases of spin-1 BECs in a 2D harmonic trap with isotropic and anisoropic SU(3) SOCs, respectively. The ground-state phases are obtained by using the time-splitting Fourier pseudospectral method with the imaginary time propagation $(t \to -\mathrm{i}t)$.[51–55] The wave function in Eq. (4) can be written as $\Psi_j(\boldsymbol{r}, t) = \sum_{k=1}^{n} \Psi_{jk}(\boldsymbol{r})\exp(-\mathrm{i}tE_k)$ $(j = -1, 0, 1)$, where $\Psi_{jk}(\boldsymbol{r})$ is the eigenfunction of the eigenvalue E_k. Each eigenfunction is attenuated by $\exp(-\mathrm{i}tE_k)$. For the different eigenfunctions, the eigenvalues E_k are different. The ground-state has the lowest energy, the decay rate

is the slowest. Therefore, after each iteration, the proportion of the ground-state becomes larger and larger. The returned wave function evolves to the ground-state wave function, and its limit is also the ground-state wave function. However, in the numerical calculation, the imaginary time propagation neither ensures the normalization nor conserves the spin-density in spin–orbit coupled spinor BECs. In order to solve this question, a backward-forward Euler Fourier-pseudospectral discretization is implemented to ensure the normalization of the total density and conservation of the spin-density. For the time discretization, we use the backward or forward Euler scheme for linear or nonlinear terms in the time derivatives. For the spatial discretization, we take fast Fourier transform in spatial derivatives. We adopt three conserved quantities to calculate the normalization constants in this paper. These quantities ensure the normalization of the total density and conservation of the spin-density after each iteration in imaginary time, the continuous normalized gradient flow has been discussed in Refs. [56,57]. In each iteration, the wave function in Eq. (4) is transformed as $\Psi_j(\boldsymbol{r},t+\Delta t)=d_j\Psi_j(\boldsymbol{r},t)$, where d_j are the normalization constants. So the constraint on the total number of atoms can be written as $N=\Sigma_j d_j^2 N_j$, where $N_j=\Sigma_{-\infty}^{\infty}|\Psi_j|^2\mathrm{d}\boldsymbol{r}$. We introduce the constraint on the spin-density as $M=\Sigma_{-\infty}^{\infty}(d_1^2|\Psi_1|^2-d_{-1}^2|\Psi_{-1}|^2)\mathrm{d}\boldsymbol{r}$. The method is discussed and used in the study of the spin–orbit coupled spin-1 and spin-2 BECs.[43,44,58–60] In our numerical simulation, the initial wave function is the normalized Gaussian wave packet, i.e., $\Psi_j(\boldsymbol{r})=(\pi\omega_r^2)^{1/4}\exp(-\boldsymbol{r}^2/2\omega_r^2)$, where ω_r is the width along the $\boldsymbol{r}$ direction. The spatial and time steps employed are $\Delta\boldsymbol{r}=0.05$ and $\Delta t=0.0001$, respectively.

In the SU(3) spin–orbit coupled spin-1 BECs, the competition between the spin–spin interaction and the isotropic SU(3) SOC plays an important role in determining the ground-state phases, a rich variety of lattice configurations are present, i.e., the PW phase, the ST phase, the KL phase, the SHL phase, and the HHL phase. The system undergoes a sequence of phase transitions from the RL phase to the HHL phase, and to the TL phase with anisotrpic SU(3) SOC.

3.1. Stripe and lattice phases with isotropic SU(3) SOC

In this section, we study the ground-state phases of the ferromagnetic and antiferromagnetic spin-1 BECs with isotropic SU(3) SOC, respectively. We first consider the ferromagnetic spin-1 BECs, i.e., $c_2<0$. The ground-state densities of spin-1 BECs with the different SOC strengths $\gamma=0$, 1, 3, and 5 are shown in Figs. 1(a)–1(d), respectively. The spin–spin interaction $c_2=-50$. The particles favor the $m_F=0$ component without SOC $\gamma=0$ in Fig. 1(a). With the SOC strength increasing, the particles begin to prefer the $m_F=\pm1$ components. As the SOC strength increases further, the densities of the three components are uniformly distributed, i.e., $|\Psi_{-1}|^2=|\Psi_0|^2=|\Psi_1|^2=N/3$, as shown in Fig. 1(d) with $\gamma=5$. For the SU(3) spin–orbit coupled ferromagnetic spin-1 BECs, the ground state is a PW phase, and one of the three minima of the single-particle energy spectrum is occupied.

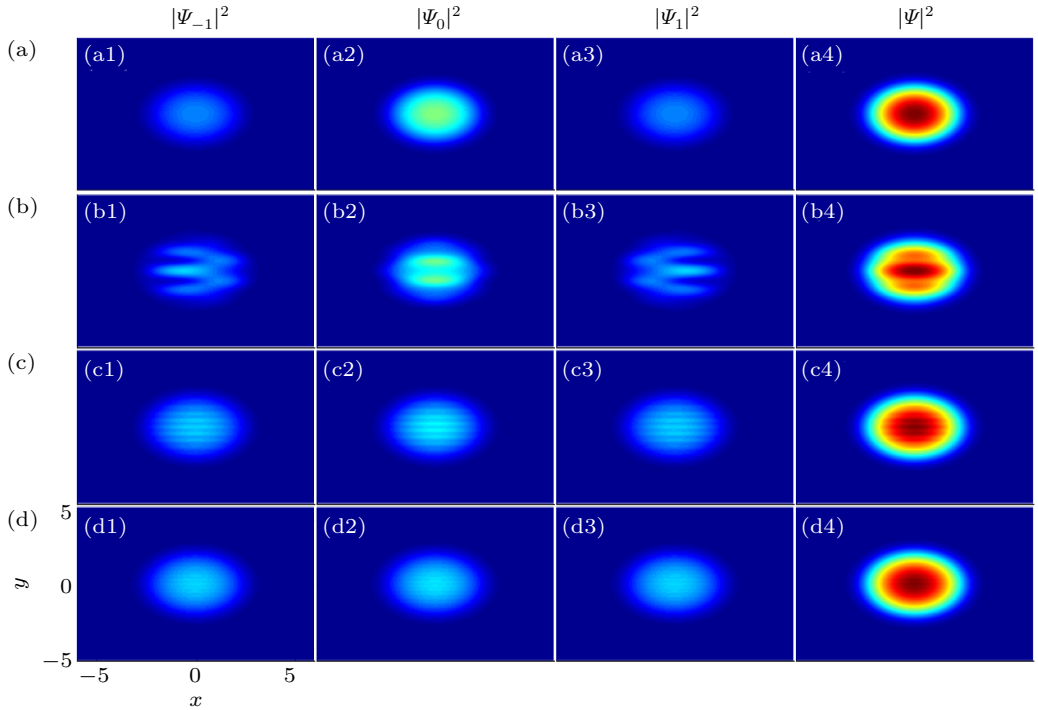


Fig. 1. The ground-state density profiles of ferromagnetic spin-1 BECs with isotropic SU(3) SOC. The columns in every panel from left to right are the densities of the $m_F=-1$ component $|\Psi_{-1}|^2$, the $m_F=0$ component $|\Psi_0|^2$, the $m_F=1$ component $|\Psi_1|^2$, and the total $|\Psi|^2=|\Psi_{-1}|^2+|\Psi_0|^2+|\Psi_1|^2$. The SOC strengths in (a)–(d) are $\gamma=0$, 1, 3, and 5, respectively. The spin–spin interaction $c_2=-50$.

Figures 2–4 exhibit the ground-state phases of antiferromagnetic spin-1 BECs with isotropic SU(3) SOC, the phenomena become interesting. The ground-state phases with the weak spin–spin interaction ($c_2 = 100$) are shown in Fig. 2. The system prefers the state that particles locate in the $m_F = \pm 1$ components evenly, i.e., $|\Psi_{-1}|^2 = |\Psi_1|^2 = N/2$, one can see in Fig. 2(a) without the SOC $\gamma = 0$. When considering the SOC, the translational symmetries of each component along the x-direction and y-direction are broken by the SOC, the densities of the three components are immiscible. The density of each component forms a kagome lattice structure[47,48] in Figs. 2(b)–2(d), we call this ground-state phase as the KL phase. Due to the presence of the strong SU(3) SOC, the momentum distribution of the KL phase has three discrete minima. The three discrete minima are occupied with the equal weights, as shown in Fig. 5(a). With the SOC strength increasing, the period of the density modulation decreases. We next discuss the ground-state phases of the SU(3) spin–orbit coupled spin-1 BECs with the large spin–spin interaction $c_2 = 2000$, a rich variety of lattice configurations are displayed. The translational symmetry of each component is broken only along one direction with the weak SOC $\gamma = 0.75$, 1.10, 1.65, as shown in Figs. 3(b)–3(d). The ground-state phases consist of alternating spin domains between $m_F = 0$ component and $m_F = \pm 1$ components, which realizes the ST phase. The ST phase is consistent with the ground-state phase of the SU(2) spin–orbit coupled spin-1 BECs. If the SOC strength is beyond a critical value ($\gamma \simeq 1.70$), the translational symmetries along both the x-direction and the y-direction are broken in each component. The double vortices structure in the total density $|\Psi|^2$ is shown in Fig. 3(e4) with the SOC strength $\gamma = 1.75$. Figures 4(a)–4(e) show the ground-state phases with the strong SOC strengths $\gamma = 2$, 2.5, 3.5, 4, and 4.4, respectively. We can find that the densities of the three components are miscible. The density of the $m_F = 0$ component has the honeycomb lattice structure and the $m_F = \pm 1$ components have the rectangular lattice structures, as shown in Fig. 4(a). The total density realizes the honeycomb lattice with a vortex core structure, which is different from the phases shown in Fig. 3. As the SOC strength increases further, the vortex core structure is replaced by the honeycomb hexagonal lattice structures in the edge regime of total densities in Figs. 4(b)–4(d). The honeycomb hexagonal lattice structure can exist stably when the SOC strength $\gamma = 4.4$ in Fig. 4(e), we take it as the HHL phase. The ground-state phases in Figs. 3(e) and 4(a)–4(d) are the transition phases between the ST phase and the HHL phase, we call them as the SHL phases.

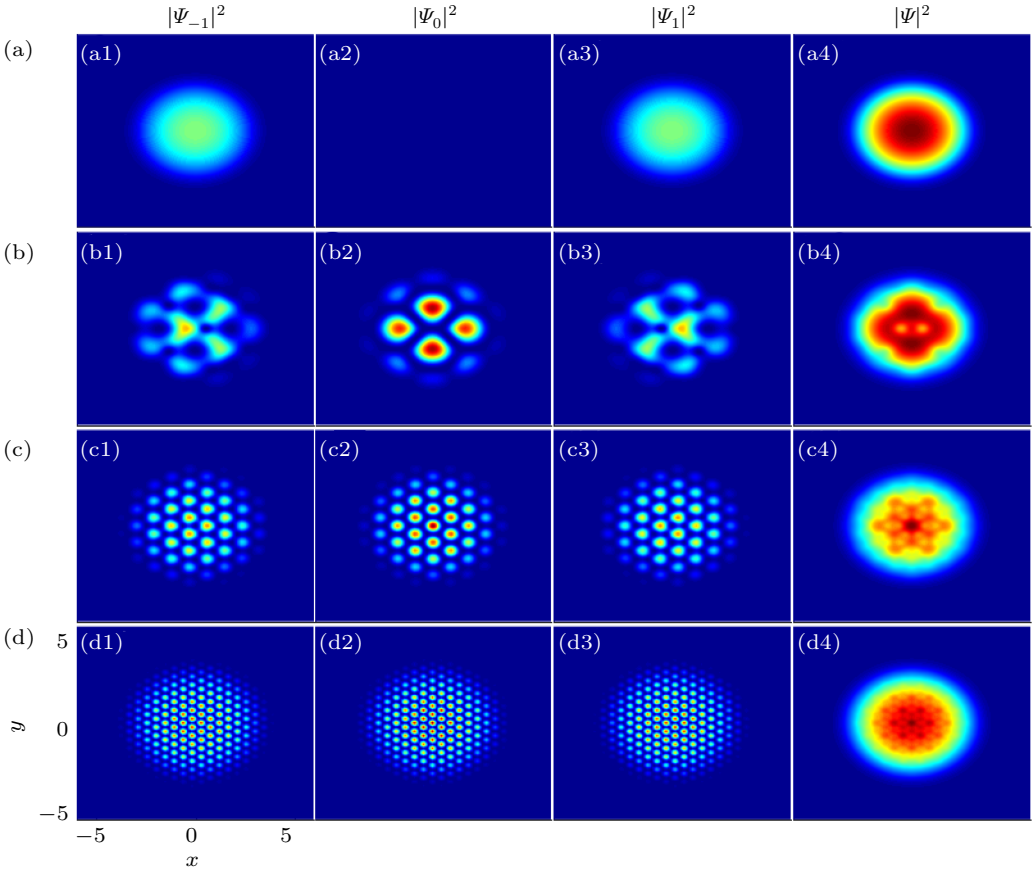


Fig. 2. The ground-state density profiles of antiferromagnetic spin-1 BECs with isotropic SU(3) SOC. The columns in every panel from left to right are the densities of the $m_F = -1$ component $|\Psi_{-1}|^2$, the $m_F = 0$ component $|\Psi_0|^2$, the $m_F = 1$ component $|\Psi_1|^2$, and the total $|\Psi|^2 = |\Psi_{-1}|^2 + |\Psi_0|^2 + |\Psi_1|^2$. The SOC strengths in (a)–(d) are $\gamma = 0$, 1, 2, and 4, respectively. The spin–spin interaction $c_2 = 100$.

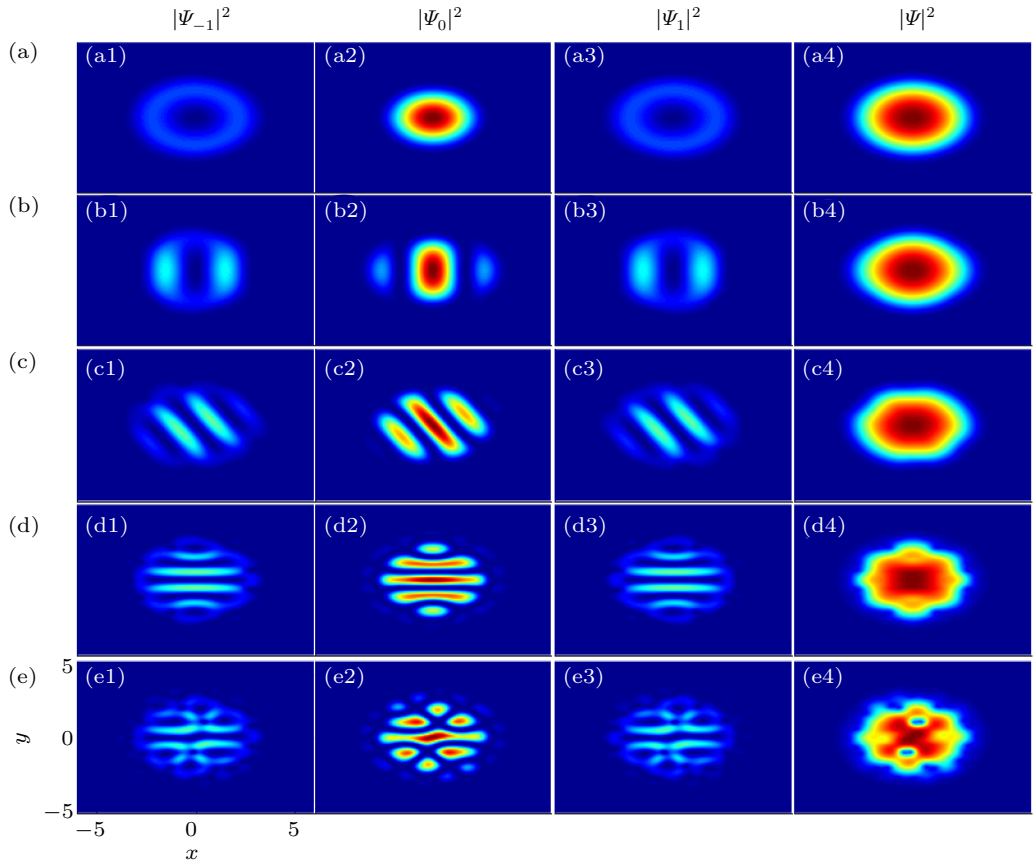


Fig. 3. The ground-state density profiles of antiferromagnetic spin-1 BECs with isotropic SU(3) SOC. The columns in every panel from left to right are the densities of the $m_F = -1$ component $|\Psi_{-1}|^2$, the $m_F = 0$ component $|\Psi_0|^2$, the $m_F = 1$ component $|\Psi_1|^2$, and the total $|\Psi|^2 = |\Psi_{-1}|^2 + |\Psi_0|^2 + |\Psi_1|^2$. The SOC strengths in (a)–(e) are $\gamma = 0.50$, 0.75, 1.10, 1.65, and 1.75, respectively. The spin–spin interaction $c_2 = 2000$.

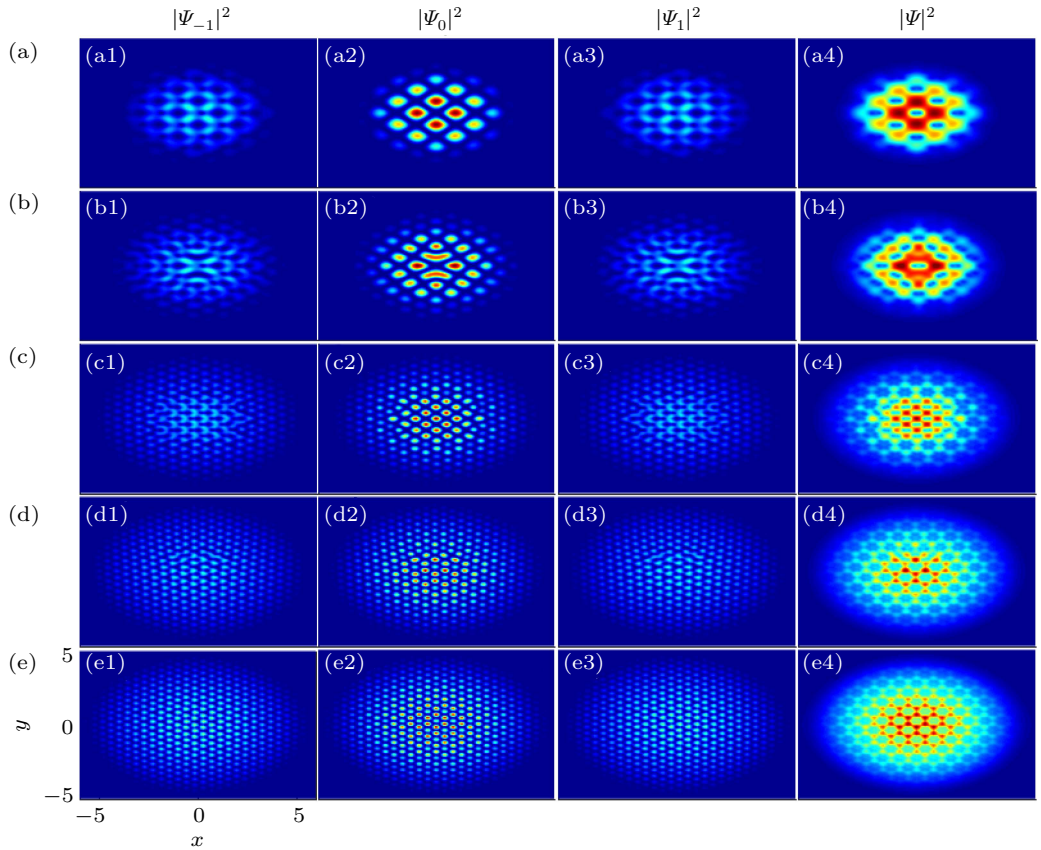


Fig. 4. The ground-state density profiles of antiferromagnetic spin-1 BECs with isotropic SU(3) SOC. The columns in every panel from left to right are the densities of $m_F = -1$ component $|\Psi_{-1}|^2$, $m_F = 0$ component $|\Psi_0|^2$, $m_F = 1$ component $|\Psi_1|^2$, and the total $|\Psi|^2 = |\Psi_{-1}|^2 + |\Psi_0|^2 + |\Psi_1|^2$. The SOC strengths in (a)-(e) are $\gamma = 2$, 2.5, 3.5, 4, and 4.4, respectively. The spin–spin interaction $c_2 = 2000$.

The momentum distributions of each component and the spin texture are shown in Fig. 5. The parameters of Figs. 5(a)–5(d) are the same as those of Figs. 2(d), 4(a), 4(b), and 4(e), respectively. The momentum distributions of each component of the KL phase (see Fig. 2(d)) show three discrete minima occupied with the equal weights in Fig. 5(a). When the SOC strength $\gamma = 2$, four discrete minima in the momentum distributions of each component are shown in the SHL phase of Fig. 5(b). The three minima of the single-particle energy spectrum are broken by the interaction and SOC, and the SHL phase with four discrete minima is a metastable state. As the SOC strength increases, one of the minima gradually weakens and eventually disappears. We find that the SHL phase with four discrete minima is confined to a very small SOC regime $1.95 \leq \gamma \leq 2.25$ in our numerical calculation. The SHL phase with three discrete minima is shown in Fig. 5(c) with the SOC strength $\gamma = 2.5$. For the HHL phase (see Fig. 4(e)), three discrete minima of the equilateral triangle have unequal weights, as shown in Fig. 5(d). The spin textures of the KL phase, the SHL phase, and the HHL phase are shown in Figs. 5(a4), 5(b4), 5(c4), and 5(d4). The spin textures show a spontaneous magnetic ordering in the form of crystals of the meron pairs and antimeron pairs with the strong SU(3) SOC strength. Previous studies indicated that stable meron-pair lattice can be obtained in two-component BECs in a periodic potential[47] or with rotation.[61] Our results show that meron-pair lattice can also be stabilized in alternating spin domains by the SU(3) SOC of spin-1 BECs.

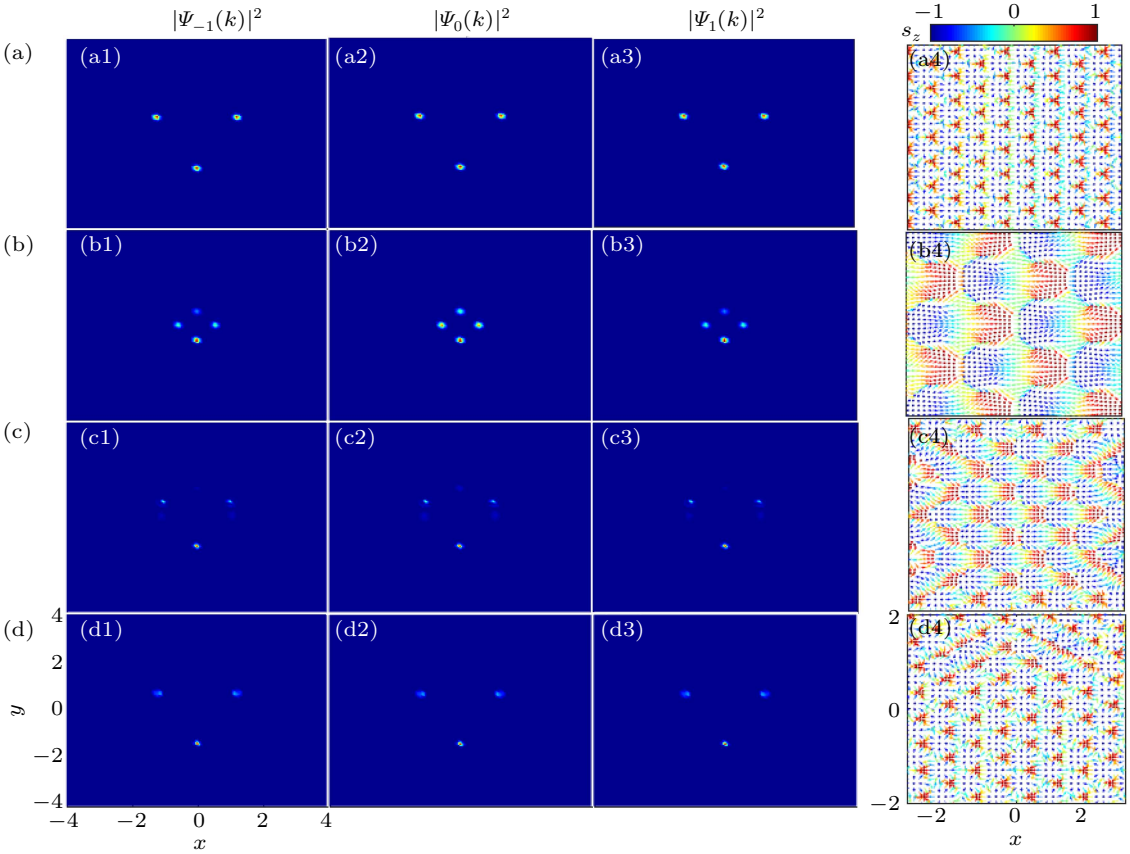


Fig. 5. The parameters of (a)–(d) are the same as those of Figs. 2(d), 4(a), 4(b), and 4(e), respectively. The momentum distributions of (b1)–(d1) the $m_F = -1$ component $|\Psi_{-1}(k)|^2$, (b2)–(d2) the $m_F = 0$ component $|\Psi_0(k)|^2$, and (b3)–(d3) the $m_F = 1$ component $|\Psi_1(k)|^2$.

The ground-state phase diagram spanned by the SU(3) SOC strength γ and the spin–spin interaction strength c_2 is shown in Fig. 6. Five ground-state phases can be identified on this phase diagram, including the PW phase, the KL phase, the SHL phase, and the HHL phase. The ferromagnetic SU(3) spin–orbit coupled spin-1 BECs ($c_2 < 0$) only have the PW phase. The PW phase is also shown in the antiferromagnetic SU(3) spin–orbit coupled spin-1 BECs ($c_2 > 0$) with the weak SOC strength $\gamma \leq 0.7$. When the spin–spin interaction strength is in the regime of $0 < c_2 \leq 600$, the system undergoes the phase transition from the ST phase to the KL phase as the SOC strength increases. With the spin–spin interaction strength c_2 increasing, the KL phase is replaced by the STL and HHL phases. The system undergoes a sequence of phase transitions from the ST phase to the STL phase, and to the HHL phase. From the phase diagram, we can find that both the spin–spin

interaction and the SU(3) SOC play an important role on the ground-state phases of the SU(3) spin–orbit coupled spin-1 BECs.

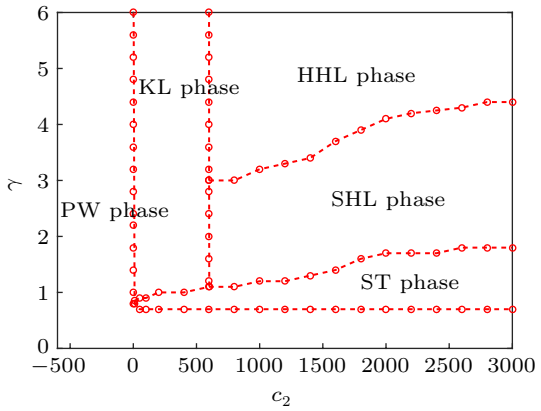


Fig. 6. The ground-state phase diagram spanned by the SU(3) SOC strength γ and the spin–spin interaction strength c_2. Five ground-state phases can be identified on the phase diagram, including the PW phase, the ST phase, the KL phase, the SHL phase, and the HHL phase.

3.2. Three types of lattice phases with anisotrpic SU(3) SOC

In order to better investigate the effect of the SU(3) SOC on the ground-state phases of spin-1 BECs, we study the ground-state phases of antiferromagnetic spin-1 BECs with anisoropic SU(3) SOC in a harmonic trap. Figure 6 exhibits the ground-state phases of anisotrpic SU(3) spin–orbit coupled spin-1 BECs with the spin–spin interaction $c_2 = 2000$ and the SOC strength along the x direction $\gamma_x = 5$. The SOC ratios in Figs. 6(a)–6(c) are $\zeta = 0.9$, 0.99, and 1.1, respectively. Three types of lattice phases are found, i.e., the RL phase, the HHL phase, and the TL phase. The translational symmetries of the total density along both the x-direction and y-direction are broken. The vortices in the neighboring chains are parallel, which form a RL phase, as shown in Fig. 6(a) with $\zeta = 0.90$. With the SOC ratio increasing, the HHL phase is shown. The HHL phase only can be found in the regime of $|\zeta - 1| \leq 0.02$. which shows that the HHL structure is the unique solution of $\zeta = 1$ in the numerical calculation. As the SOC ratio increases further, the translational symmetries of the total density along the x-direction and y-direction are also broken, the vortices of the neighboring chains are stagger. The TL phase is found in Fig. 6(c) with $\zeta = 1.1$. The translational symmetry is broken by the SOC ratio, and the system undergoes a sequence of phase transitions from the RL phase to the HHL phase, and to the TL phase in spin-1 BECs with anisotrpic SU(3) SOC.

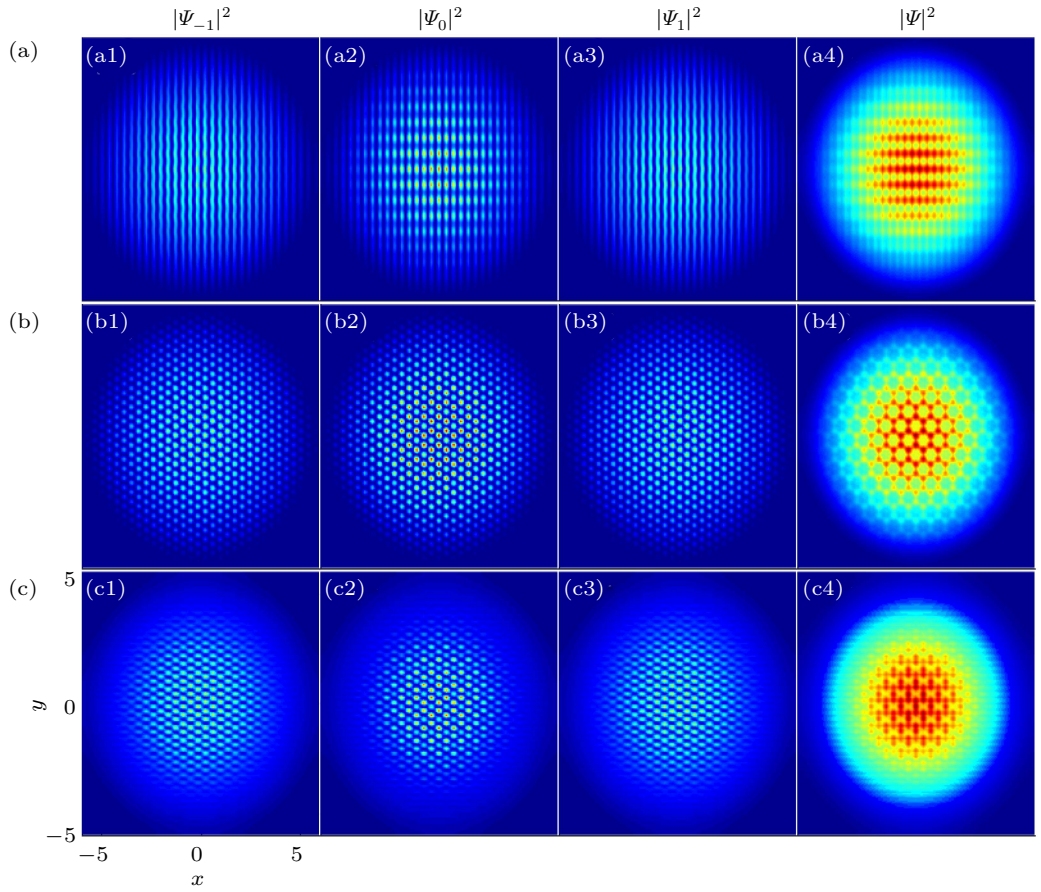


Fig. 7. The ground-state density profiles of spin-1 antiferromagnetic BECs with anisotropic SU(3) SOC. The columns in every panel from left to right are the densities of $m_F = -1$ component $|\Psi_{-1}|^2$, $m_F = 0$ component $|\Psi_0|^2$, $m_F = 1$ component $|\Psi_1|^2$, and the total $|\Psi|^2 = |\Psi_{-1}|^2 + |\Psi_0|^2 + |\Psi_1|^2$. The SOC ratios in (a)–(c) are $\zeta = 0.90$, 0.99 and 1.1, respectively. The spin–spin interaction $c_2 = 2000$ and the SOC strength along the x direction $\gamma_x = 5$.

4. Summary

We have investigated the ground-state phases of 2D isotropic and anisotropic SU(3) spin–orbit coupled spin-1 BECs in a harmonic trap respectively. The competition between the SU(3) SOC and spin–spin interaction results in a rich variety of lattice configurations. Five ground-state phases, i.e., the PW phase, the ST phase, the KL phase, the SHL phase, and the HHL phase, are identified on the phase diagram with isotropic SU(3) SOC. The system undergoes a sequence of phase transitions from the RL phase to the HHL phase, and to the TL phase in spin-1 BECs with anisotrpic SU(3) SOC.

References

[1] Lin Y J, Compton R L, Perry A R, Phillips W D, Porto J V and Spielman I B 2009 *Phys. Rev. Lett.* **102** 130401
[2] Lin Y J, Compton R L, Jiménez-García K, Porto J V and Spielman I B 2009 *Nature* **462** 628
[3] Lin Y J, Jiménez-García K and Spielman I B 2011 *Nature* **471** 83
[4] Lin Y J, Compton R L, Jiménez-García K, Phillips W D, Porto J V and Spielman I B 2011 *Nat. Phys.* **7** 531
[5] Anderson B M, Juzeliunas G, Galitski V M and Spielman I B 2012 *Phys. Rev. Lett.* **108** 235301
[6] Wu Z, Zhang L, Sun W, Xu X T, Wang B Z, Ji S C, Deng Y, Chen S, Liu X J and Pan J W 2016 *Science* **354** 83
[7] Huang L, Meng Z, Wang P, Peng P, Zhang S L, Chen L, Li D, Zhou Q and Zhang J 2016 *Nat. Phys.* **12** 540
[8] Sun W, Wang B Z, Xu X T, Yi C R, Zhang L, Wu Z, Deng Y, Liu X J, Chen S and Pan J W 2018 *Phys. Rev. Lett.* **121** 150401
[9] Wang C, Gao C, Jian C M and Zhai H 2010 *Phys. Rev. Lett.* **105** 160403
[10] Wu C and Mondragon-Shem I 2011 *Chin. Phys. Lett.* **28** 097102
[11] Li Y, Pitaevskii L P and Stringari S 2012 *Phys. Rev. Lett.* **108** 225301
[12] Chen X, Rabinovic M, Anderson B M and Santos L 2014 *Phys. Rev. A* **90** 043632
[13] Wilson R M, Anderson B M, and Clark C W 2013 *Phys. Rev. Lett.* **111** 185303
[14] Achilleos V, Frantzeskakis D J, Kevrekidis P G and Pelinovsky D E 2013 *Phys. Rev. Lett.* **110** 264101
[15] Kasamatsu K 2015 *Phys. Rev. A* **92** 063608
[16] Zhang D W, Fu L B, Wang Z D and Zhu S L 2012 *Phys. Rev. A* **85** 043609
[17] Xu Y, Zhang Y P and Wu B 2013 *Phys. Rev. A* **87** 013614
[18] Sakaguchi H, Li B and Malomed B A 2014 *Phys. Rev. E* **89** 032920
[19] Zhong R X, Chen Z P, Huang C Q, Luo Z H, Tan H S, Malomed B A and Li Y Y 2018 *Front. Phys.* **13** 130311
[20] Li Y Y, Zhang X L, Zhong R X, Luo Z H, Liu B, Huang C Q, Pang W, Malomed B A 2019 *Commun Nonlinear Sci Numer Simulat* **73** 481
[21] Ho T L 1998 *Phys. Rev. Lett.* **81** 742
[22] Ciobanu C V, Yip S K and Ho T L 2000 *Phys. Rev. A* **61** 033607
[23] Song J L, Semenoff G W and Zhou F 2007 *Phys. Rev. Lett.* **98** 160408
[24] Turner A M, Barnett R, Demler E and Vishwanath A 2007 *Phys. Rev. Lett.* **98** 190404
[25] Martone G I, Pepe F V, Facchi P, Pascazio S and Stringari S 2016 *Phys. Rev. Lett.* **117** 125301
[26] Campbell D L, Price R M, Putra A, Valdés-Curiel A, Trypogeorgos D and Spielman I B 2016 *Nat. Commun.* **7** 10897
[27] Luo X, Wu L, Chen J, Guan Q, Gao K, Xu Z F, You L and Wang R 2016 *Sci. Rep.* **6** 18983
[28] Wen L, Sun Q, Wang H Q, Ji A C and Liu W M 2012 *Phys. Rev. A* **86** 043602
[29] Lan Z H and Öhberg P 2014 *Phys. Rev. A* **89** 023630
[30] Natu S S, Li X P and Cole W S 2015 *Phys. Rev. A* **91** 023608
[31] Sun K, Qu C L, Xu Y, Zhang Y P and Zhang C W 2016 *Phys. Rev. A* **93** 023615
[32] Yu Z Q 2016 *Phys. Rev. A* **93** 033648
[33] Hurst H M, Wilson J H, Pixley J H, Spielman I B and Natu S S 2016 *Phys. Rev. A* **94** 063613
[34] Wang J G, Xu L L and Yang S J 2017 *Phys. Rev. A* **96** 033629
[35] Huang X Y, Sun F X, Zhang W, He Q Y and Sun C P 2017 *Phys. Rev. A* **95** 013605
[36] Wang J G and Yang S J 2018 *J. Phys.: Condens. Matter* **30** 295404
[37] Wang J G and Yang S J 2018 *Eur. Phys. J. Plus* **133** 441
[38] Peng P, Li G Q, Zhao L C, Yang W L and Yang Z Y 2019 *Phys. Lett. A* **383** 2883
[39] Xu Z F, Lü R and You L 2011 *Phys. Rev. A* **83** 053602
[40] Kawakami T, Mizushima T and Machida K 2011 *Phys. Rev. A* **84** 011607
[41] Wang J G, Wang W and Yang S J 2019 *Phys. Lett. A* **383** 566
[42] Wan N S, Li Y E and Xue J K 2019 *Phys. Rev. E* **99** 062220
[43] Gautam S and Adhikari S K 2015 *Phys. Rev. A* **91** 013624
[44] Gautam S and Adhikari S K 2015 *Phys. Rev. A* **91** 063617
[45] Grab T, Chhajlany R W, Muschik C A and Lewenstein M 2014 *Phys. Rev. B* **90** 195127
[46] Barnett R, Boyd G R and Galitski V 2012 *Phys. Rev. Lett.* **109** 235308
[47] Han W, Zhang X F, Song S W, Saito H, Zhang W, Liu W M and Zhang S G 2016 *Phys. Rev. A* **94** 033629
[48] Li H and Chen F L 2019 *Chin. Phys. B* **28** 070302
[49] Yue H X and Liu Y K 2020 *Commun. Theor. Phys.* **72** 025501
[50] Kawaguchi Y and Ueda M 2012 *Phys. Rep.* **520** 253
[51] Bao W, Jin S and Markowich P A 2002 *J. Comput. Phys.* **175** 487
[52] Bao W, Jaksch D and Markowich P A 2003 *J. Comput. Phys.* **187** 318
[53] Bao W, Jaksch D and Markowich P A 2004 *Multiscale Model. Simul.* **2** 210
[54] Bao W, Chern I L and Zhang Y Z 2013 *J. Comput. Phys.* **253** 189
[55] Wang H 2007 *Int. J. Comput. Math.* **84** 925
[56] Lim F Y and Bao W 2008 *Phys. Rev. E* **78** 066704
[57] Bao W and Lim F Y 2008 *Siam J. Sci. Comp.* **30** 1925
[58] Gautam S and Adhikari S K 2014 *Phys. Rev. A* **90** 043619
[59] Gautam S and Adhikari S K 2017 *Phys. Rev. A* **95** 013608
[60] Peng P, Li G Q, Yang W L and Yang Z Y 2018 *Phys. Lett. A* **382** 2493
[61] Kasamatsu K, Tsubota M, and Ueda M 2004 *Phys. Rev. Lett.* **93** 250406